Detecting Topological Phases in Cold Atoms

Xiong-Jun Liu,[1,2,3] K. T. Law,[2] T. K. Ng,[2] and Patrick A. Lee[1]

[1]*Department of Physics, Massachusetts Institute of Technology, Cambridge, Massachusetts 02139, USA*
[2]*Department of Physics, Hong Kong University of Science and Technology, Clear Water Bay, Hong Kong, China*
[3]*Institute for Advanced Study, Hong Kong University of Science and Technology, Clear Water Bay, Hong Kong, China*

(Received 2 July 2013; published 20 September 2013)

Chern insulators are band insulators which exhibit a gap in the bulk and gapless excitations in the edge. Detection of Chern insulators is a serious challenge in cold atoms since the Hall transport measurements are technically unrealistic for neutral atoms. By establishing a natural correspondence between the time-reversal invariant topological insulator and the quantum anomalous Hall system, we show for a class of Chern insulators that the topology can be determined by only measuring Bloch eigenstates at highly symmetric points of the Brillouin zone. Furthermore, we introduce two experimental schemes, including the spin-resolved Bloch oscillation, to carry out the measurement. These schemes are highly feasible under realistic experimental conditions. Our results may provide a powerful tool to detect topological phases in cold atoms.

DOI: 10.1103/PhysRevLett.111.120402 PACS numbers: 03.65.Vf, 37.10.Jk, 67.85.−d

The recent great advancement in realizing synthetic spin-orbit (SO) coupling [1–6] turns cold atom systems into new and promising platforms to probe exotic topological phases beyond natural conditions [7–9]. So far, the experimentally realized SO interaction [2–6] is a one-dimensional (1D) SO term with equal Rashba and Dresselhaus amplitudes through a two-photon Raman process as proposed by an earlier theoretical work [1]. The study of higher dimensional topological phases necessitates the realization of higher dimensional SO interactions in the cold atoms [10–16]. While a 2D or 3D synthetic SO term is yet to be realized in experiment, theoretical schemes have been proposed [17–19]. In particular, it was proposed in a very recent work that the 2D SO interaction can be realized with realistic cold atom platforms [20]. In the single particle regime, this model describes a quantum anomalous Hall (QAH) insulator (Chern insulator) [21] which exhibits a gap in the bulk and chiral edge modes in the boundary [22–25].

Because of the absence of local orders, topological phases are typically hard to detect. For cold atoms, the task may be even more demanding since quantized (Hall) transport measurements [26], widely exploited in the solid state systems, are technically unrealistic for neutral atoms. On the other hand, while the detection of gapless edge modes by, e.g., the light Bragg scattering proposed in Ref. [23], is in principle straightforward, its usefulness may be limited by the difficulty in separating edge state signals from the bulk background and complicated by realistic boundary conditions [27–29]. Alternative strategies for the detection include to measure the state-dependent atom density response to an external field [30], the bulk Chern number from Berry curvature over the Brillouin zone (BZ) [31,32], Zak's phase [33], and charge pumping [34]. While these methods provide direct detection of the bulk topological invariants, they rely on complicated manipulations or measurements on the whole bulk band, which may still be challenging for the delicate cold atom systems.

In this Letter, we propose to detect Chern insulators by measuring the bulk states at only a few highly symmetric points of the BZ. By establishing a natural correspondence between the time-reversal (TR) invariant topological insulator and the QAH system, we show for a class of Chern insulators that the topology can be determined by measuring the Bloch eigenstates at only highly symmetric points of the BZ. This greatly simplifies measurement in the realistic experiments. We further introduce experimental schemes, including the spin-resolved Bloch oscillation in 2D optical lattices, to carry out the measurement of the topological states.

We consider the square optical lattice model for spin-1/2 cold atoms proposed in a recent work, which has essential advantages in its experimental realization [20]. The main results of this Letter, as shown below and detailed in the Supplemental Material [35], can be applied to more general Chern insulators and lattice configurations, including honeycomb lattices. The Hamiltonian of the system $H = \sum_{\mathbf{k},\sigma\sigma'} \hat{c}^{\dagger}_{\mathbf{k},\sigma} \mathcal{H}_{\sigma,\sigma'}(\mathbf{k}) \hat{c}_{\mathbf{k},\sigma'}$, with

$$\mathcal{H}(\mathbf{k}) = d_x(\mathbf{k})\sigma_x + d_y(\mathbf{k})\sigma_y + d_z(\mathbf{k})\sigma_z, \qquad (1)$$

where $d_z = m_z - 2t_0\cos(k_x a) - 2t_0\cos(k_y a)$ and $d_{x,y} = -2t_{\mathrm{SO}}\sin(k_{y,x}a)$, with m_z a controllable Zeeman splitting induced by a small two-photon off resonance in the Raman couplings and t_0 and $t^{(0)}_{\mathrm{SO}}$ representing the nearest-neighbor spin-conserved and spin-flipped hopping coefficients, respectively [20]. In the cold atom context, spin refers to two hyperfine levels. The topology of the system is characterized by the first Chern number expressed by the

integral of the Berry curvature over the first BZ: $C_1 = (1/2\pi)\int dk_x dk_y \mathcal{B}_{-,z}(\mathbf{k})$, where $\mathcal{B}_{\pm}(\mathbf{k}) = \nabla_{\mathbf{k}} \times \mathcal{A}_{\pm}(\mathbf{k})$ and $\mathcal{A}_{\pm}(\mathbf{k}) = i\hbar\langle u_{\pm,\mathbf{k}}|\nabla_{\mathbf{k}}|u_{\pm,\mathbf{k}}\rangle$, with $|u_{\pm,\mathbf{k}}\rangle$ labeling the upper and lower Bloch eigenstates solved from the Hamiltonian (1). Direct calculation shows that $C_1 = \mathrm{sgn}(m_z)$ when $0 < |m_z| < 4t_0$, and otherwise $C_1 = 0$.

A Chern insulator explicitly breaks TR symmetry. Nevertheless, the above Hamiltonian H is symmetric under the 2D inversion transformation defined by $P = \hat{P} \otimes \hat{R}_{2\mathrm{D}}$, where $\hat{P} = \sigma_z$ acting on spin space and the 2D spatial operator $\hat{R}_{2\mathrm{D}}$ transforms the Bravais lattice vector $\mathbf{R} \to -\mathbf{R}$. For the Bloch Hamiltonian, we have $\hat{P}\mathcal{H}(\mathbf{k})\hat{P}^{-1} = \mathcal{H}(-\mathbf{k})$, which follows that at the four highly symmetric points $[\hat{P}, \mathcal{H}(\mathbf{\Lambda}_i)] = 0$, with $\{\mathbf{\Lambda}_i\} = \{(0,0), (0,\pi), (\pi,0), (\pi,\pi)\}$. Therefore, the Bloch states $|u_{\pm}(\mathbf{\Lambda}_i)\rangle$ are also eigenstates of the parity operator $\hat{P}$, with eigenvalues $\xi_i^{(\pm)} = +1$ or -1. Similarly to topological insulators [36,37], we define the following invariant

$$(-1)^{\nu} = \prod_i \xi^{(-)}(\mathbf{\Lambda}_i) \tag{2}$$

and can verify for Hamiltonian (1) that $\nu = 0$ when the system is in the trivial regime and $\nu = 1$ for the topological regime. Furthermore, for the present square lattice, which has four Dirac points coinciding with the four highly symmetric points, the Chern number is given by

$$C_1 = -\frac{\nu}{2}\sum_i \xi^{(-)}(\mathbf{\Lambda}_i). \tag{3}$$

It is straightforward to check that when the Zeeman term varies from $m_z \gtrsim 0$ to $m_z \lesssim 0$, two parity eigenvalues $\xi^{(-)}_{\mathbf{\Lambda}_2,\mathbf{\Lambda}_3}$ change sign and then C_1 changes from 1 to -1.

For a more general Hamiltonian with inversion symmetry, we demonstrate below and show in more detail in the Supplemental Material [35] that when ν given by Eq. (2) is 1, the Chern number is odd and the system is nontrivial, while for $\nu = 0$, the number C_1 is even and the system may or may not be nontrivial. The essential idea is to adopt the topological classification of a TR variant topological insulator which can be artificially constructed from the studied Chern insulator and its time-reversed artificial copy. Following the Fu-Kane theorem (see the Supplemental Material for more details [35]), the topological invariant of a 2D TR invariant topological insulator with inversion symmetry can be determined by the product of the four parity eigenvalues, as given in Eq. (2) [36,37]. Note that the TR invariant topological insulator is constructed by two independent time-reversed copies of Chern insulators. Generically, the *trivial* ($\nu = 0$) and *topological* ($\nu = 1$) phases of the TR invariant topological insulator, respectively, correspond to the *even* and *odd* Chern numbers for the two copies of QAH insulators. Therefore, the invariant given by Eq. (2) exactly describes the topology of a Chern insulator when $|C_1|$ is either 0 or 1, which is true for most of the available theoretical models in cold atoms [22–25,27–33].

The formula (2) is the central result of this work to be applied to the detection of Chern insulators which preserve parity symmetry and satisfy $|C_1| = \{0, 1\}$. Note that for a cold atom system, the possible values of C_1 can be exactly known by theory. Since only the four parity eigenstates at $\mathbf{k} = \mathbf{\Lambda}_i$ need to be measured, the procedure of detecting a Chern insulator can be essentially simplified. In the rest of this Letter, we study two different approaches based on Bloch oscillation [38,39] to detect the Chern insulating phases given by the Hamiltonian (1). Note that Eq. (2) can apply to other lattice configurations such as honeycomb lattices, with new results predicted [35]. Also, these results are valid for both fermions and bosons trapped in the 2D optical lattice.

First, we consider to measure the topological invariants from the Berry curvature $\mathcal{B}_+ = -\mathcal{B}_-$ at the four symmetric points. A straightforward calculation yields that

$$\mathcal{B}_- = \left[\frac{2m_z t_{\mathrm{SO}}^2}{d^3(\mathbf{k})}\cos k_x \cos k_y - \frac{4t_s t_{\mathrm{SO}}^2}{d^3(\mathbf{k})}(\cos k_x + \cos k_y)\right]\hat{e}_z, \tag{4}$$

with $d(\mathbf{k}) = [\sum_j d_j^2(\mathbf{k})]^{1/2}$. It can be verified that $\mathrm{sgn}[\mathcal{B}_{-,z}(0,\pi)] = \mathrm{sgn}[\mathcal{B}_{-,z}(\pi,0)] = \mathrm{sgn}[\xi^{(-)}_{0,\pi}] = \mathrm{sgn}[\xi^{(-)}_{\pi,0}]$ and $\mathrm{sgn}[\mathcal{B}_{-,z}(0,0)] = -\mathrm{sgn}[\mathcal{B}_{-,z}(\pi,\pi)] = -\mathrm{sgn}[\xi^{(-)}_{0,0}] = \mathrm{sgn}[\xi^{(-)}_{\pi,\pi}]$, which follows that $\prod_i \mathrm{sgn}[\mathcal{B}_{-,z}(\mathbf{\Lambda}_i)] = \prod_i \xi^{(-)}(\mathbf{\Lambda}_i)$. Therefore, measuring $\xi^{(-)}(\mathbf{\Lambda}_i)$ reduces to measuring $\mathrm{sgn}(\mathcal{B}_{-,z})$ at the four momenta $\mathbf{k} = \mathbf{\Lambda}_i$, which can be carried out by Bloch oscillation. We emphasize that the present approach is essentially different from that in Ref. [32], which suggests to detect the bulk Chern number by measuring quantitatively $\mathcal{B}_-$ over the BZ. Here, only the signs of $\mathcal{B}_{-,z}$ at four points need to be measured. Note that we always have $\mathcal{B}^-_{0,\pi} = \mathcal{B}^-_{\pi,0}$. The measurement can be further simplified to determine $\mathcal{B}_-$ at $\mathbf{\Lambda}_1 = (0,0)$ and $\mathbf{\Lambda}_4 = (\pi,\pi)$. In the presence of an external force $\mathbf{F} = F_x\vec{e}_x + F_y\vec{e}_y$ in the x-y plane, which can be set by ramping the optical trapping or chirping the lattice frequency [39], the Bloch wave packet oscillates along the direction of the force, while it deflects to the transverse direction due to the Berry curvature. The deflection direction provides a straightforward measurement of the sign of the Berry curvature.

The semiclassical dynamics of a wave packet at band n ($= \pm$) with center-of-mass position $\mathbf{r}_c$ and momentum $\mathbf{k}_c$ is given by $\hbar\dot{\mathbf{k}}_c = \mathbf{F}(\mathbf{r}_c)$ and $\dot{\mathbf{r}}_c = \mathbf{v}_{0n} - \mathbf{F} \times \mathcal{B}_n(\mathbf{k}_c)$, where $\mathbf{v}_{0n} = \hbar^{-1}\partial_{\mathbf{k}}\mathcal{E}_n(\mathbf{k})$ and $\mathcal{E}_n(\mathbf{k})$ is the dispersion relation. The second term in the equation of $\dot{\mathbf{r}}_c$ represents the anomalous velocity, leading to the transverse shift. Note that the transverse shift in a unit Bloch time

$$\Delta\mathbf{r}_c = -\int_0^{2\pi} d\mathbf{k}_c \times \mathcal{B}_n(\mathbf{k}_c)$$

is independent of the force strength but sensitive to the magnitude of Berry curvature. To make the results easily distinguishable in realistic experiments, an appreciable transverse shift is preferred, which can be achieved by tuning m_z close to the phase transition points. In particular, to measure $\mathcal{B}_{0,0}$ and $\mathcal{B}_{\pi,\pi}$, we can tune m_z close to $4t_0$ and $-4t_0$, in which cases the transverse shift is dominated by the Berry curvature around $\mathbf{\Lambda}_1$ and $\mathbf{\Lambda}_4$, respectively. The signs of $\mathcal{B}_{0,0}$ and $\mathcal{B}_{\pi,\pi}$ are directly read out from directions of the transverse shift.

In the realistic experiment, one shall consider a cloud of cold atoms which are initially trapped by a harmonic optical potential and centered at $\mathbf{r}_0 = 0$. The square lattice potentials are adiabatically switched on, along with the switch-off of the harmonic trap, and the atoms populate the states at the band bottom (for bosons) or starting from the band bottom (for fermions) [39]. Applying the static force $\mathbf{F}$ in the 2D plane accelerates the atomic cloud, with the dynamics described by the distribution function $\rho_{\pm}(\mathbf{r}, \mathbf{k}, T, \tau)$, where T is the temperature. The initial profile of the atomic cloud, determined by $\rho_{\pm}(\mathbf{r}, \mathbf{k}, T, 0)$, can be adjusted by the optical trapping potentials before switching on the square lattice. For the case of a weak force satisfying that $\pi E_g^2 \gg 2at_{\mathrm{SO}}|\mathbf{F}|$ with E_g the band gap, we can neglect the Landau-Zener (LZ) transition between the lower to upper subbands [40]. The evolution of $\rho_{\pm}(\mathbf{r}, \mathbf{k}, T, \tau)$, governed by the semiclassical Boltzmann equation, satisfies the ballistic law and reads

$$\rho_{\pm}(\mathbf{r}, \mathbf{k}, T, \tau) = \rho_{\pm}\Big(\mathbf{r} - \int_0^{\tau} \mathbf{v}_{0\pm} dt' + \int_0^{\tau} \mathbf{F} \times \mathcal{B}_{\pm}(\mathbf{k}) dt', \mathbf{k} - \int_0^{\tau} dt' \mathbf{F}/\hbar, T, 0\Big). \quad (5)$$

With this solution, the dynamics of the atomic cloud can be studied numerically, as presented below.

The Berry curvatures $\mathcal{B}_{0,0}$ and $\mathcal{B}_{\pi,\pi}$ are determined from the numerical simulation in Fig. 1, where we plot the atomic density at zero temperature $n_-(\mathbf{r}, \tau) = \int d^2\mathbf{k} \rho_-(\mathbf{r}, \mathbf{k}, 0, \tau)$ with its maximum magnitude rescaled to be unit. Note that the band bottom of the lower subband is located at $\mathbf{k}_{\mathrm{bot}} = (\pi, \pi)$ for $m_z > 0$ and at $\mathbf{k}_{\mathrm{bot}} = (0, 0)$ if $m_z < 0$. By applying $\mathbf{F}$ in the $\hat{e}_{x'} = (\hat{e}_x + \hat{e}_y)/\sqrt{2}$ direction, the atomic cloud oscillates in the position space along this direction while it deflects to the transverse $\pm\hat{e}_{y'} = \pm(\hat{e}_y - \hat{e}_x)/\sqrt{2}$ direction due to the Berry curvature. By tuning the Zeeman parameter m_z from less than to greater than $4t_0$, we can see that the transverse motion changes from the $-\hat{e}_{y'}$ to the $+\hat{e}_{y'}$ direction [Figs. 1(a) and 1(b)], which implies that $\mathcal{B}_{0,0}$ changes direction from the $-z$ to the $+z$ direction. On the other hand, by tuning m_z from $m_z > -4t_0$ to $m_z < -4t_0$, the transverse motion changes from the $+\hat{e}_{y'}$ to the $-\hat{e}_{y'}$ direction, again implying that $\mathcal{B}_{\pi,\pi}$ changes from the $+z$ to the $-z$ direction [Figs. 1(c) and 1(d)]. With these results, one gets that $\nu = 1$ for $0 < |m_z| < 4t_0$ and $\nu = 0$ for $|m_z| \geq 4t_0$, and the topological phase is obtained in the former regime. Similar phenomena can be obtained for Berry curvatures $\mathcal{B}_{\mathbf{\Lambda}_2}$ and $\mathcal{B}_{\mathbf{\Lambda}_3}$ by tuning m_z close to zero (not shown here). In this way, we further find that $C_1 = \mathrm{sgn}(m_z)$ in the topological phase.

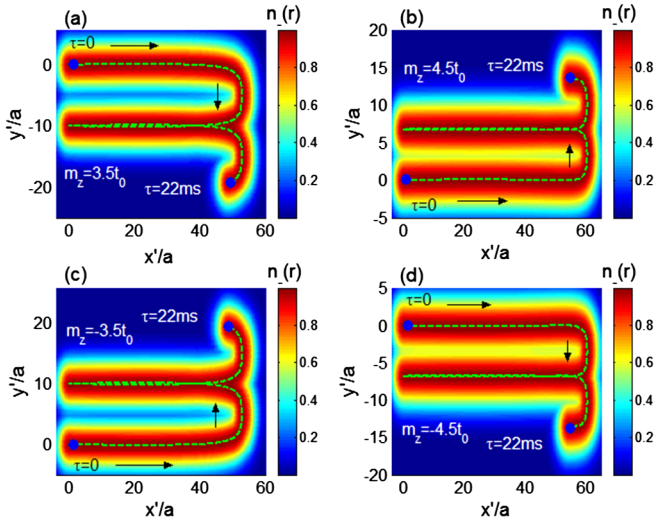

FIG. 1 (color online). Measuring $\mathrm{sgn}(\mathcal{B}_{-,z})$ at (a), (b) $\mathbf{\Lambda}_1 = (0, 0)$ and at (c),(d) $\mathbf{\Lambda}_4 = (\pi, \pi)$ by Bloch oscillation, which determines the topology of the bulk band. The static force, applied along the $\hat{e}_{x'} = (\hat{e}_x + \hat{e}_y)/\sqrt{2}$ direction, induces transverse deflection of the atomic cloud to $\pm\hat{e}_{y'} = \pm(\hat{e}_y - \hat{e}_x)/\sqrt{2}$. Other parameters are taken as $t_{\mathrm{SO}} = t_0 = 2\pi \times 0.52$ kHz [20] and $|\mathbf{F}| = 0.13t_0/a$.

Now, we introduce another approach for the measurement: the spin-resolved Bloch oscillation. We shall determine the topology of the bulk by measuring the spin polarization of the atomic cloud at the highly symmetric points. Note for the present square lattice the parity operator $\hat{P} = \sigma_z$, so the parity eigenstates are simply the spin eigenstates, with the spin-up and spin-down corresponding to different hyperfine levels. It then follows that $\prod_i \xi^{(-)}(\mathbf{\Lambda}_i) = \prod_i \mathrm{sgn}[p_{\mathrm{spin}}(\mathbf{\Lambda}_i)]$, where the

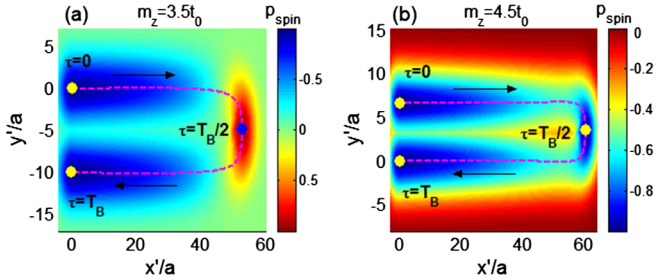

FIG. 2 (color online). Spin-resolved Bloch oscillation with the force along the $\hat{e}_{x'}$ direction. (a) Topological regime with $m_z = 3.5t_0$. The spin polarization $\mathrm{sgn}[p_{\mathrm{spin}}(0)] = -\mathrm{sgn}[p_{\mathrm{spin}}(T_B/2)]$. (b) Trivial regime with $m_z = 4.5t_0$. The spin polarization $\mathrm{sgn}[p_{\mathrm{spin}}(0)] = \mathrm{sgn}[p_{\mathrm{spin}}(T_B/2)]$.

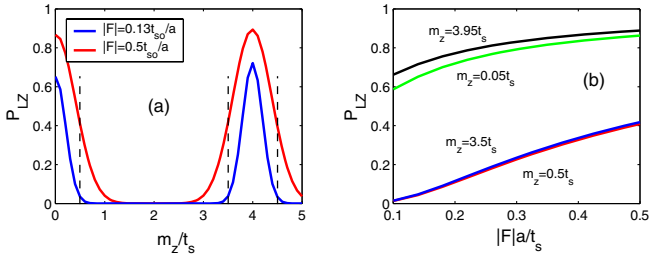

FIG. 3 (color online). Landau-Zener probability P_{LZ} for the atomic cloud evolving through the avoided band crossing point, as a function of (a) m_z and of (b) $|\mathbf{F}a|$. For the numerical calculation, the initial atomic cloud has a narrow momentum distribution with radius relative to the central momentum (at the band bottom) about $k_{\mathrm{rad}} \simeq 0.2/a$.

spin-polarization density $p_{\mathrm{spin}} = (n_\uparrow - n_\downarrow)/n_-$ with $n_{\uparrow/\downarrow}$ the spin-up or -down component of the atomic density and $n_- = n_\uparrow + n_\downarrow$. The spin polarization can be measured directly in experiment by imagining the densities of atoms in two different hyperfine levels. Similarly, since the polarizations for the states at $\mathbf{k} = \mathbf{\Lambda}_2$ and $\mathbf{k} = \mathbf{\Lambda}_3$ are the same, the bulk topology is determined by $\mathrm{sgn}(p_{\mathrm{spin}})$ at $\mathbf{k} = \mathbf{\Lambda}_1$ and $\mathbf{k} = \mathbf{\Lambda}_4$.

In Fig. 2, we numerically plot the spin-polarization density $p_{\mathrm{spin}}(\tau)$ in the Bloch oscillation with $\mathbf{F}$ along the $\hat{e}_{x'}$ direction. For the case $0 < m_z < 4t_0$, the spin polarization of the atomic cloud, starting with the center momentum $\mathbf{k} = (0, 0)$, changes from $p_{\mathrm{spin}} \simeq -1$ at $\tau = 0$ to $p_{\mathrm{spin}} \simeq 1$ at half Bloch time $\tau = T_B/2$, and then reverses back to $p_{\mathrm{spin}} \simeq -1$ again when a unit Bloch period is finished at $\tau = T_B$ [Fig. 2(a)]. The sign change of the spin polarization in a unit Bloch oscillation tells us that $\nu = 1$, and the mass terms exhibit opposite signs for the Dirac equations around $\mathbf{\Lambda}_1 = (0, 0)$ and $\mathbf{\Lambda}_4 = (\pi, \pi)$, so the system is in the topological phase. Figure 2(b) shows that in the case $m_z \geq 4t_s$, the spin polarization $p_{\mathrm{spin}} < 0$ for the whole Bloch oscillation, and therefore the phase is trivial. The results for $m_z < 0$ are similar. With these phenomena, one can again determine that the topological phase is obtained when $0 < |m_z| < 4t_0$, with the Chern number $C_1 = \mathrm{sgn}(m_z)$. It is noteworthy that the spin-resolved Bloch oscillation does not require a large transverse shift in the Bloch oscillation and thus can be more straightforward for experimental studies.

So far, we have considered the weak static force regime. In the opposite parameter regime with $\pi E_g^2 < 2at_{\mathrm{SO}}|\mathbf{F}|$, the LZ transition between the lower and higher subbands must be taken into account when the center-of-mass momentum of the atomic cloud is accelerated to the avoided crossing point [40]. For convenience, we denote that $\mathbf{k} = (k_\perp, k_\parallel)$ with $k_\perp$ and $k_\parallel$ the momenta perpendicular and parallel to $\mathbf{F}$, respectively. Since $k_\perp$ is unchanged, it is useful to define $\tilde{E}_g(k_\perp) = \min[\mathcal{E}_+(k_\perp)]$ as the minimum of the upper subband energy with fixed $k_\perp$. Then, a state

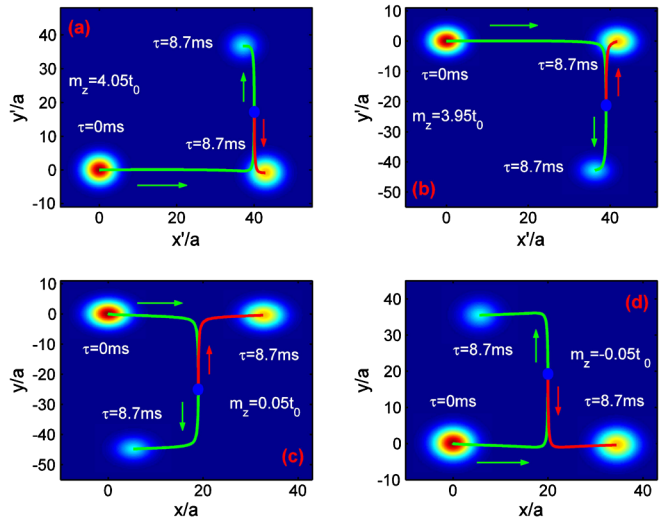

FIG. 4 (color online). Atomic cloud splitting induced by the LZ transition close to the phase transition points. A tiny bulk gap opens at $\mathbf{k} = \mathbf{\Lambda}_1$ for (a) $m_z = 4.05t_0$ and (b) $m_z = 3.95t_0$, and at $\mathbf{k} = \mathbf{\Lambda}_2, \mathbf{\Lambda}_3$ for (c) $m_z = 0.05t_0$ and (d) $m_z = -0.05t_0$, with the magnitude of the gap $E_g = 0.05t_0$. Other parameters are taken as $t_{\mathrm{SO}} = t_0 = 2\pi \times 0.52$ kHz, and the force $|\mathbf{F}| = 0.2t_0/a$ applied along the (a),(b) $\hat{e}_{x'}$ and the (c),(d) $\hat{e}_x$ directions, respectively. The arrows represent the directions of atomic cloud motion.

initially at a lower band and with momentum $\mathbf{k}$ transitions to the upper band with the LZ probability $\bar{p}(k_\perp) = e^{-\pi \tilde{E}_g^2(k_\perp)/(v_F|\mathbf{F}|)}$ [40]. The averaging transition probability is given by $P_{\mathrm{LZ}} = \int d^2\mathbf{r}d^2\mathbf{k}\rho_-(\mathbf{r}, \mathbf{k})\bar{p}(k_\perp)/\int d^2\mathbf{r}n_-(\mathbf{r})$, with numerical results shown in Fig. 3 for different parameter regimes.

The LZ transition leads to the splitting of the atomic cloud from one to two, which provides a detection of the critical point of the topological phase transition. The numerical results are shown in Fig. 4. For the cases with $m_z \gtrsim 4t_s$ [Fig. 4(a)] and $m_z \lesssim 4t_s$ [Fig. 4(b)], a tiny bulk gap is located at $\mathbf{\Lambda}_1 = (0, 0)$. Applying the static force along the $\hat{e}_{x'}$ direction, we can see that the atomic cloud first is deflected to the $\hat{e}_{y'}$ [for (a)] or the $-\hat{e}_{y'}$ [for (b)] direction and then splits into two when the central momentum is accelerated to the $\mathbf{\Lambda}_1$ point. The atomic cloud corresponding to the lower subband keeps the original deflection route, while the new cloud formed by the atoms in the upper band states is deflected oppositely, reflecting that $\mathcal{B}_\pm$ are opposite in the z direction. Similarly, by tuning $m_z \sim 0$, one can detect the phase transition due to the gap closing at $\mathbf{\Lambda}_2$ and $\mathbf{\Lambda}_3$ by applying the force along the $\hat{e}_x$ (or the $\hat{e}_y$) direction [Figs. 4(c) and 4(d)].

In conclusion, we proposed to detect 2D Chern insulators by measuring the bulk states at four highly symmetric points of the BZ. From a natural correspondence between the TR invariant topological insulator and the QAH system, we show for a class of Chern insulators that the topology can be determined by measuring the parity eigenstates at only highly symmetric points of the BZ.

Moreover, the detection relies on only qualitative rather than quantitative measurements on physical numbers. This enables a much simpler strategy to detect the topological phases comparing with conventional methods to measure the edge states or bulk Chern invariants. We further introduced two realistic experimental schemes to carry out the measurement, and our detection strategy can be applied to both square and honeycomb lattice systems, the two most relevant configurations for the cold atom experiments [35]. It is noteworthy that these schemes can also be directly applied to the detection of TR invariant topological insulators. Our work showcases the advantages of cold atoms since the parity eigenstates are hard to directly measure in a condensed matter system. Our results can provide a powerful tool to detect topological phases in cold atoms.

We thank Waseem Bakr, Lawrence W. Cheuk, Wujie Huang, Tin-Lun Ho, Liang Fu, and Junwei Liu for very helpful discussions. We acknowledge support from HKRGC through Grants No. 605512 and No. HKUST3/CRF09. P. A. L. acknowledges support by DOE Grant No. DE-FG-02-03-ER46076.

[1] X.-J. Liu, M. F. Borunda, X. Liu, and J. Sinova, Phys. Rev. Lett. **102**, 046402 (2009).
[2] Y.-J. Lin, K. Jiménez-García, and I. B. Spielman, Nature (London) **471**, 83 (2011).
[3] M. Chapman and C. Sá de Melo, Nature (London) **471**, 41 (2011).
[4] L. W. Cheuk, A. T. Sommer, Z. Hadzibabic, T. Yefsah, W. S. Bakr, and M. W. Zwierlein, Phys. Rev. Lett. **109**, 095302 (2012).
[5] P. Wang, Z.-Q. Yu, Z. Fu, J. Miao, L. Huang, S. Chai, H. Zhai, and J. Zhang, Phys. Rev. Lett. **109**, 095301 (2012).
[6] J.-Y. Zhang *et al.*, Phys. Rev. Lett. **109**, 115301 (2012).
[7] Kangjun Seo, Li Han, and C. A. R. Sá de Melo, Phys. Rev. Lett. **109**, 105303 (2012).
[8] X.-J. Liu, Z.-X. Liu, and M. Cheng, Phys. Rev. Lett. **110**, 076401 (2013).
[9] V. Galitski and I. B. Spielman, Nature (London) **494**, 49 (2013).
[10] X.-J. Liu, X. Liu, L. C. Kwek, and C. H. Oh, Phys. Rev. Lett. **98**, 026602 (2007); Phys. Rev. B **79**, 165301 (2009).
[11] C. Zhang, S. Tewari, R. M. Lutchyn, and S. Das Sarma, Phys. Rev. Lett. **101**, 160401 (2008).
[12] M. Sato, Y. Takahashi, and S. Fujimoto, Phys. Rev. Lett. **103**, 020401 (2009).
[13] J. P. Vyasanakere and V. B. Shenoy, Phys. Rev. B **83**, 094515 (2011); J. P. Vyasanakere, S. Zhang, and V. B. Shenoy, *ibid.* **84**, 014512 (2011).
[14] W. Yi and G.-C. Guo, Phys. Rev. A **84**, 031608(R) (2011); L. He and X.-G. Huang, Phys. Rev. Lett. **108**, 145302 (2012); F. Wu, G.-C. Guo, W. Zhang, and W. Yi, *ibid.* **110**, 110401 (2013).
[15] L. Dell'Anna, G. Mazzarella, and L. Salasnich, Phys. Rev. A **86**, 053632 (2012).
[16] Q. Zhou and X. Cui, Phys. Rev. Lett. **110**, 140407 (2013).
[17] J. Ruseckas, G. Juzeliunas, P. Ohberg, and M. Fleischhauer, Phys. Rev. Lett. **95**, 010404 (2005).
[18] C. Zhang, Phys. Rev. A **82**, 021607(R) (2010).
[19] D. L. Campbell, G. Juzeliūnas, and I. B. Spielman, Phys. Rev. A **84**, 025602 (2011).
[20] X.-J. Liu, K. T. Law, and T. K. Ng, arXiv:1304.0291.
[21] F. D. M. Haldane, Phys. Rev. Lett. **61**, 2015 (1988).
[22] C. Wu, Phys. Rev. Lett. **101**, 186807 (2008).
[23] X.-J. Liu, X. Liu, C. Wu, and J. Sinova, Phys. Rev. A **81**, 033622 (2010).
[24] M. Zhang, H.-H. Hung, C. Zhang, and C. Wu, Phys. Rev. A **83**, 023615 (2011); S.-S. Zhang, H. Fan, and W.-M. Liu, Phys. Rev. A **87**, 023622 (2013).
[25] P. Hauke *et al.*, Phys. Rev. Lett. **109**, 145301 (2012).
[26] C.-Z. Chang *et al.*, Science **340**, 167 (2013).
[27] N. Goldman, J. Beugnon, and F. Gerbier, Phys. Rev. Lett. **108**, 255303 (2012).
[28] M. Buchhold, D. Cocks, and W. Hofstetter, Phys. Rev. A **85**, 063614 (2012).
[29] N. Goldman, J. Dalibard, A. Dauphin, F. Gerbier, M. Lewenstein, P. Zoller, and I. B. Spielman, Proc. Natl. Acad. Sci. U.S.A. **110**, 6736 (2013).
[30] L. B. Shao, S.-L. Zhu, L. Sheng, D. Y. Xing, and Z. D. Wang, Phys. Rev. Lett. **101**, 246810 (2008).
[31] E. Alba, X. Fernandez-Gonzalvo, J. Mur-Petit, J. K. Pachos, and J. J. Garcia-Ripoll, Phys. Rev. Lett. **107**, 235301 (2011).
[32] H. M. Price and N. R. Cooper, Phys. Rev. A **85**, 033620 (2012).
[33] D. A. Abanin, T. Kitagawa, I. Bloch, and E. Demler, Phys. Rev. Lett. **110**, 165304 (2013).
[34] L. Wang, A. A. Soluyanov, and M. Troyer, Phys. Rev. Lett. **110**, 166802 (2013).
[35] See Supplemental Material at http://link.aps.org/supplemental/10.1103/PhysRevLett.111.120402 for more details.
[36] L. Fu and C. L. Kane, Phys. Rev. B **74**, 195312 (2006).
[37] L. Fu and C. L. Kane, Phys. Rev. B **76**, 045302 (2007).
[38] L. Tarruell, D. Greif, T. Uehlinger, G. Jotzu, and T. Esslinger, Nature (London) **483**, 302 (2012); L.-K. Lim, J.-N. Fuchs, and G. Montambaux, Phys. Rev. Lett. **108**, 175303 (2012).
[39] O. Morsch and M. Oberthaler, Rev. Mod. Phys. **78**, 179 (2006).
[40] C. Zener, Proc. R. Soc. A **137**, 696 (1932); L. D. Landau, Phys. Z. **2**, 46 (1932).